Precision Engineering 60 (2019) 535–543

Contents lists available at ScienceDirect

Precision Engineering

journal homepage: www.elsevier.com/locate/precision

Kinematic mirror mount design for ultra-precision manufacturing, metrology, and system level integration for high performance visible spectrum imaging systems

Nicholas W. Horvath *, Matthew A. Davies, Steven R. Patterson

University of North Carolina at Charlotte, Department of Mechanical Engineering, 9201 University City Blvd., Duke Centennial Hall, Charlotte NC 28223, USA

ARTICLE INFO

Keywords:
Exact constraint design
Kinematic coupling
Repeatability
Freeform optics
Metrology
Kinematic mount
Ultra precision machining
Single point diamond turning

ABSTRACT

High-performance freeform optical systems, designed for broad spectral imaging from the visible to the far infrared, place new demands on optical design, precision manufacturing, and precision metrology. To meet the tolerances on figure, roughness, and relative positioning in such systems requires the ability to perform metrology and manufacturing corrections on freeform optics in a continuous feedback loop. This feedback loop requires a common interface for machining and manufacturing platforms. This paper describes the design, analysis, and testing of such an interface suitable for use with single point diamond turning and deterministic micro-grinding. The interface utilizes a torsionally preloaded, robust, kinematic mount capable of supporting manufacturing process loads while maintaining the position repeatability in five degrees of freedom required for the measurement and correction of optical figure. Results from a prototype system demonstrate absolute in-plane position uncertainty less than 200 nm and 50 nm, respectively, and axial position uncertainty is 40 nm absolute and 10 nm relative. The absolute and relative angular positioning uncertainties less than 1 μrad and 0.25 μrad respectively. The results exceed the requirements for many optical systems. The mount is also suitable for use in opto-mechanical assembly, so that the same platform can be used for manufacturing, metrology, final assembly, testing, and service.

1. Introduction

High performance visible spectrum optical systems that operate in a variety of changing conditions require a deterministic approach to the design and manufacture of each critical component. The use of freeform optics can reduce overall volume while maintaining performance [1], with the trade-off of increased sensitivity and tighter tolerances. Freeform surfaces also require sub aperture manufacturing processes such as single point diamond turning (SPDT), magnetorheological finishing (MRF), and deterministic micro-grinding. These processes produce error patterns, typically manifesting as waviness or mid-spatial frequencies, that are not typically seen in traditional optics manufacturing. Further, freeform metrology platforms with uncertainties less than the manufacturing platform are needed to correct and validate optical components [2]. Thus, the use of freeforms introduces new challenges that must be dealt with in the manufacturing-metrology loop.

Ideally, a feedback loop between metrology and manufacturing is implemented to determine when the process has reached figure convergence, and an independent metrology platform is used to validate the results [3]. In order to appropriately measure the figure of the optic, reference features such as datums and fiducials are required to establish a local coordinate system. These reference features must not only be realizable in manufacturing and metrology but also at the system level. During assembly and optical testing, datums and fiducials allow the measurable positioning of each optic relative to the previous in all six degrees of freedom with controlled tolerances. In this paper, we focus on the design for manufacture and metrology, but recognize that for high performance optical systems, datums and fiducials must also be realizable during assembly and testing. Thus, the mechanical interface described in this paper is designed not only to provide a common interface between manufacturing and metrology platforms, but also to provide a high precision interface between each optic and the system housing.

Tolerances in freeform optical systems are demanding and meeting them requires and iterative process to mitigate the effects of machine motion and thermal errors in ultraprecision manufacturing equipment. During the in-process iterative feedback loop between manufacturing and metrology, the optic must be repeatedly remounted on the

* Corresponding author.
E-mail address: Nhorvat1@uncc.edu (N.W. Horvath).

https://doi.org/10.1016/j.precisioneng.2019.09.011
Received 29 April 2019; Received in revised form 9 September 2019; Accepted 18 September 2019
Available online 20 September 2019

manufacturing and metrology equipment with sub-micrometer level positioning accuracy, typically requiring custom fixturing [4]. In order to achieve figure accuracy, the mounting stresses and associated deformations must also be minimized. Exact constraint designs, such as a kinematic mount or kinematic coupling [5], is a well-known technique for mounting components that achieves these goals.

In an exact constraint design, the number of constraints equal the number of rigid-body degrees of freedom in a system. An example is the three ball, three vee groove kinematic coupling [6]. If the contact interfaces are assumed to be point contacts with zero friction, then a theoretical perfect constraint with perfect position repeatability is obtained. However, in reality deformations and friction exist at the interfaces, and because the size and shape of the contact patches are functions of the contact forces, both coupling stiffness and repeatability will also be a function of loading conditions. Using Hertzian contact theory, one can model each constraint location to determine the displacement, stiffness, and stress at the mounting interface as a function of preload. From this, the joint compliance as a function of loads coming from both preload and process load can be determined.

A common trade off in an exact constraint mount is that increased load capacity typically leads to degraded positioning repeatability. Several designs have been developed to balance this trade off. Culpepper described a quasi kinematic coupling with a theoretical line contact at the interfaces. This design provided a moderate load capacity with 0.5 μm repeatability at relatively low cost [7]. An alternate approach was discussed by Willoughby [8] and Slocum [6] to provide a large load support while maintaining a near point contact and associated repeatability. In this approach, two sections of a sphere are joined to produce a "canoe ball" or "canoe". When interfaced with a vee the deformations of the "canoe" result in a high aspect ratio elliptical contact patch, effectively distributing the load to reduce the risk of plastic deformation while maintaining sub-micron repeatability. A drawback with this design is the cost of the "canoe" shaped component which is manufactured with a high precision contouring grinder [8]. Coupling repeatability has been covered both analytically and experimentally for many designs, some of which show the direct effect of preload on system repeatability [5,8,9].

In the present work, the authors detail the design of a kinematic mount that maintains position repeatability suitable for the manufacture of freeform optics while supporting the loads expected in precision manufacturing. The design has several advantages over others previously reported [6,10–13]. First, it does not require expensive strict tolerances on the kinematic mount components themselves [14]. Second, it provides moderate load support, and third, it is demonstrated to have sub-micron repeatability. The design leverages some previous work in the field, specifically the understanding of effective groove angle and its effect on repeatability due to friction and preload [9]. A primary goal of the design is to maintain a minimum stiffness during single point diamond turning (SPDT) or deterministic micro-grinding while simultaneously maintaining sub-micrometer positioning repeatability. This paper describes the design, analysis, and experimental performance of the kinematic coupling. Through modeling the effect of process forces on stiffness is predicted and used to set the preload forces to maintain the stiffness at a desired level. The mount utilizes a novel torsional preload produced magnetically and is suitable for rapid mounting and dismounting on metrology and manufacturing platforms, thus closing the manufacturing and metrology loop needed for the deterministic manufacture of freeform optics.

2. Mount design

2.1. System and mount load conditions

The mirror mount design is driven by a diffraction limited off-axis multi-mirror visible spectrum imaging system with a set of specific load cases [15]. During operation, the instrument will experience temperature variation, must operate in arbitrary orientations, and survive high-g accelerations in any orientation. The surface figure error on the mirror must be less than 100 nm RMS during operation to maintain performance. While the design of the lightweighted mirror to maintain this performance is out of the scope of this document, the constraint design and overview of the mirror assembly is shown. In order to meet the required specification of the instrument, the final mirrors will be made in silicon carbide (SiC) with a CVD SiC cladding on the optical surface.

To generate the freeform surface in SiC, a process known as deterministic micro-grinding must be used [16]. During this process, a diamond grit resin-bonded grinding wheel is used to grind the surface with depths of cuts on the order of 1 μm during finishing operations. This document is constrained to showing the aluminum prototypes of the mirrors, which are direct replicas of the SiC mirrors, with a nickel phosphorus coating for diamond turning.

Along with the system level load cases, manufacturing and metrology of the mirrors impose load conditions and constraints. Considering the manufacture and metrology as part of the load conditions, then some additional drivers are identified as reduced packaging, robustness, manufacturing forces, accessible datums, and sub-micrometer position repeatability. For this reason, the effect from the process force magnitudes during manufacturing were modeled to verify the stiffness of the mount. Also, the design details how a definable coordinate system was created for the optical surface that can be transferred between the manufacturing platform, metrology, and then integrated into the instrument.

2.2. Mount configuration

An optic is paired with an optical cell, whose design is used for both the manufacturing mount and application mount. The optical cell has the appropriate reference datums to establish a coordinate system for the optic. These datums also act as the mating interface features at the system-level. The optic is installed on a set of kinematic mounts, allowing for removal of the optic for in-process intermittent metrology. Stated in Section 1, to meet the figure tolerance of the optical prescription, the mirror would have to be manufactured and then measured on separate metrology equipment. Therefore, there is an uncertainty in the position of the optic relative to the optical cell which can affect performance of the instrument after completion of the optical surface. The system-level error budget for the instrument accounted for the peak to valley repeatability targets, initially 1 μm for the linear degrees of freedom (x, y, z) and 10 μrad for the rotational degrees of freedom (ϵ_x, ϵ_y).

The design of the mount comprises three identical kinematic joints, equally-spaced on a circle, at 66 percent the diameter of the optic. Equally-spaced identical joints provide an athermal mount configuration, where a change in temperature will allow for a nominally uniform change in size while maintaining position of the vertex. The exact constraint design reduces the risk of optical surface deformation from external forces, where the errors will largely be rigid body motions of the optic.

Each joint is rotated 90 degrees about the coupling angle bisectors and provides constraint in the axial and azimuthal directions, requiring a torsional preload, Fig. 1. The bisector represents a degree of freedom, thus rotation of each joint will still maintain an exact constraint configuration. This technique of rotating a groove or set of grooves about the bisector has been shown by Slocum generically for a vertical configuration [6] and by Hale on the National Ignition Facility at Lawrence Livermore National Lab mirror mounts [13]. While groove rotations to support a mirror for a vertical configuration has been shown, to the author's knowledge, this paper is the first to detail a design and prototype for a torsionally preloaded kinematic mirror mount.

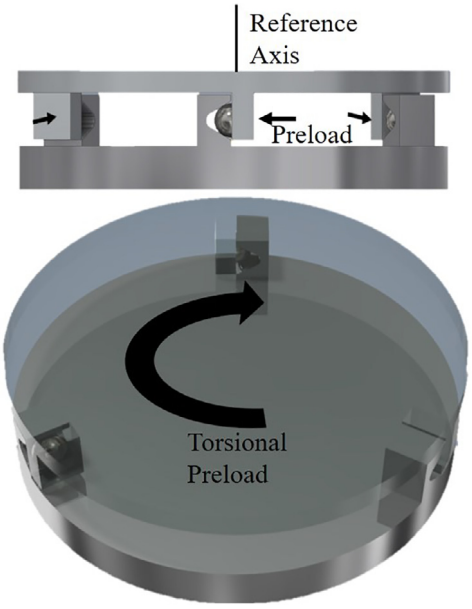

Fig. 1. A generic representation of a torsionally preloaded kinematic coupling, with the mounting locations shown near the diameter for clarity.

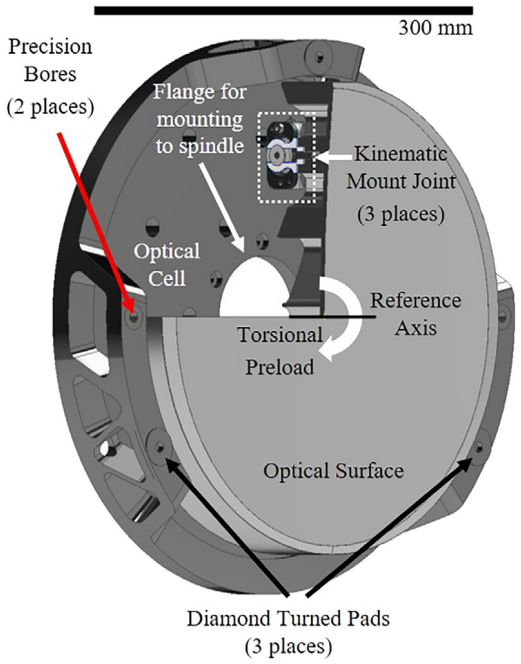

Fig. 2. The optical cell comprises a flange that mounts the optical cell to the spindle nose of the diamond turning machine. The optic is installed in the optical cell by a torsionally preloaded kinematic mount and the freeform optical surface is diamond turned in coordinated axis mode. Three pads and two bores on the optical cell are diamond turned and milled, respectively, to establish a coordinate system on the optical cell. The coordinate system of the optic and freeform optical surface is relative to the optical cell. The three pads and two precision bores locate the optical cell, and therefore the optical surface, into the global coordinate system of the imaging instrument.

In this configuration, the preload direction is perpendicular to the reference axis of the optic, requiring a rotation of the optic to seat the mount. Preload in each joint is set by a permanent magnet with an adjustment to change distance between the magnet and mating component. Fig. 2 shows the final design of the optic, paired with the optical cell, and kinematic mount assembly. The novelty of this design is two fold, where the configuration intrinsically reduces the concern of the mirror decoupling from the optical cell due to an arbitrary gravity vector, thus, satisfying the high-g survival load condition. Also, during manufacturing, the normal force from the rake face of the diamond turning tool or the feed direction during micro grinding is in the same direction as the preload force, therefore nominally increasing the stiffness of the mount.

2.3. Manufacturing configuration

The optical cell is mounted to the spindle nose of the ultra precision diamond turning machine. To create a measurable coordinate system on the optical cell, the central bore inside the flange and three interface pads are single point diamond turned, defining the z-axis and origin, and rotations about the x-axis and y-axis. The optical cell is rotated by the spindle to align the freeform prescription. Precision bores are diamond milled in the optical cell along a defined axis of the prescription, which completes the datum definition of all 6 degrees of freedom for the optical cell. The three pads and two precision bores are later used for locating the optical cell and optic into the global coordinate system of the imaging instrument.

The optic is installed on the kinematic mount and the diameter and a freeform orientation flat are SPDT or ground. The purpose of the defined diameter and orientation flat are for coarse optic alignment on separate metrology equipment for initial figure measurement. The optical surface is manufactured in coordinated axis mode (c–x–z) with the vertex of the optic set as an integer number of millimeters from the 3 diamond turned pads on the optical cell. Once the final pass on the optical surface is completed, the 3 pads on the optical cell are recut to set the axial distance of the optic relative to the optical cell. This technique removes the initial position offsets present from the kinematic mount assembly, pairing the optic and optical cell for life. The completion of this process results in a fully definable coordinate system for the optical surface, with the optical cell as the reference.

The optic is then removed from the kinematic mount and the optical cell remains on the spindle of the diamond turning machine. The optic is installed on a matched kinematic mount on a separate machine for figure metrology. For this stage of metrology, the references required are only the turned diameter and orientation flat. Piston and tilt errors from the metrology mount can be removed during data processing. If the figure tolerance is not met, the optic is reinstalled in the optical cell on the manufacturing platform and is corrected. This process redefines the 3 pad reference features at each iteration until figure convergence is achieved. Once figure specification is met, the optical surface location uncertainty relative to the optical cell, is given by the uncertainty in the repeatability of the kinematic mount, which was quantified and documented in this paper.

2.4. Description of components

The kinematic mount plane was designed near the shear plane of an lightweighted optic, shown in Fig. 3. This reduces angular effects at the optical surface from arbitrary gravity loading orientations and forces during manufacturing. It also reduces the bending moment due to friction in the joint. Fig. 3 also shows the location of an eccentric pin that changes the gap of the magnetic preload. The pin access allows for easy preload adjustment in any configuration. When the magnet is at the maximum gap distance, the preload force is approximately 5 N per joint, holding the optic in place until the user rotates it out of the seat. A joint from the prototype kinematic mount installed on the optic is shown in Fig. 4.

Fig. 5 contains the component details of one kinematic joint. Component 1 is an ogive with a 100 mm radius at the mating interface in one cross section and a 9 mm radius in a perpendicular cross section. Component 2 is a truncated cylinder pair with a 50 mm radius. The design creates an elliptical contact patch, distributing the load and

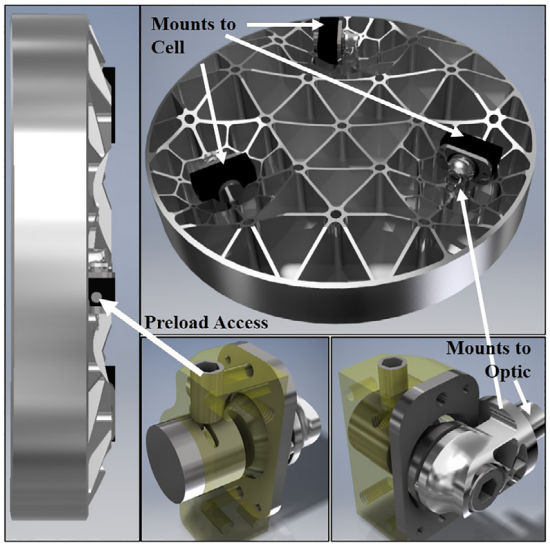

Fig. 3. Model of lightweighted optic with kinematic joints installed. The joints are also shown, one component transparent to show internal detail of component interactions.

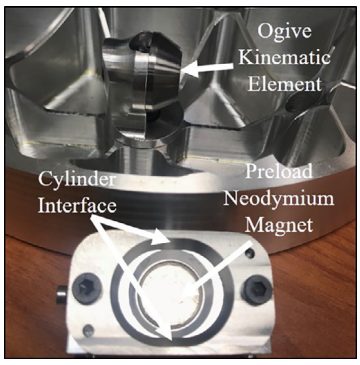

Fig. 4. Prototype Kinematic joint disconnected.

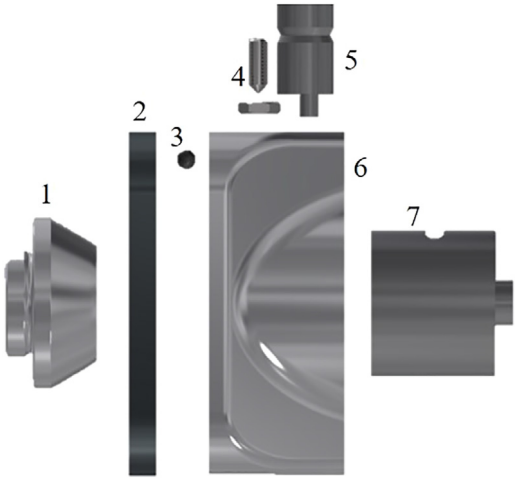

Fig. 5. Component detailed view.

reducing the contact stresses. The details of the interface are shown in Table 1 and the general description is shown in Fig. 6.

The design of the geometry allowed for a traditional manufacturing process, where component 1 was turned on a Milltronics CNC Lathe and Component 2 was ground flat and machined on a Makino A51 CNC

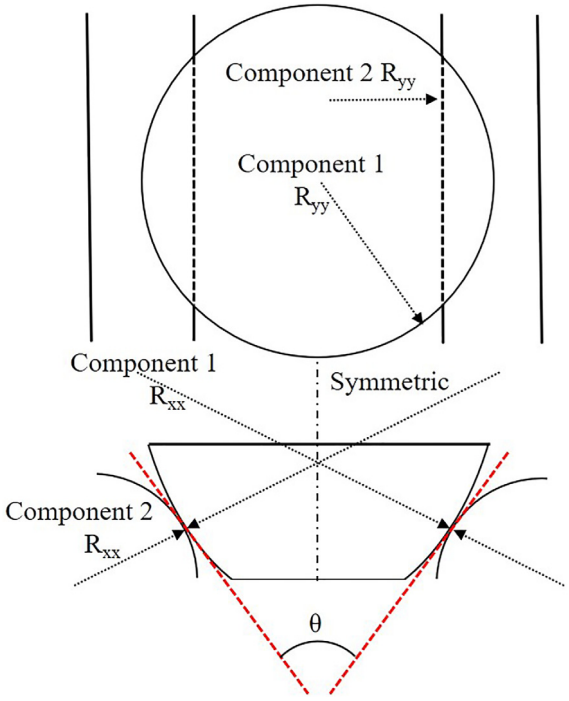

Fig. 6. Schematic representation of the interface between Component 1 and Component 2.

Table 1
Kinematic mount component contact details with an effective groove angle of 58° and a preload of 65 N.

	Component 1	Component 2
Radius	R_{xx} = 100 mm	R_{xx} = 50 mm
Radius	R_{yy} = 9 mm	R_{yy} = infinity
Contact patch dimensions	183 μm x 78 μm	183 μm x 78 μm
Max pressure	533 MPa	533 MPa
Max shear	105 MPa	105 MPa

Mill, after which the groove was lightly burnished. The material used for both components was 17-4 PH stainless steel.

Component 3–7 provide the mechanics for the joint. Components 5 and 7 are inserted into Component 6, Component 5 fitting into a slot of Component 7. Components 3 and 4 constrain Component 5 from being removed from Component 6 yet allowing a rotational degree of freedom. Rotation of component 5 will cause a linear translation of Component 7. The translation changes the gap between the magnet in component 7 and the face of Component 1. The maximum force in this system is applied when component 7 rests on the seat in Component 6. Component 1 mounts to the optic and Component 6 mounts to the optical cell. Because the optic is initially manufactured to a near net shape and requires post processing once combined as an assembly with the optical cell, each Component, including the optic and optical cell only required standard machining tolerances, on the order of 100 μm.

2.5. Coupling stiffness

The stiffness of the mount is a function of the loading force applied to each joint. The loading force comes from the preload and, in manufacturing, is also affected by process forces. Therefore, it is important to understand how the process forces affect the "net preload" and hence the stiffness of each joint. To do this, we apply tangential and normal process force components, F_t and F_n on the optical surface, project the forces into the kinematic mount grooves and look at the effect of force location on the net preload, and therefore stiffness.

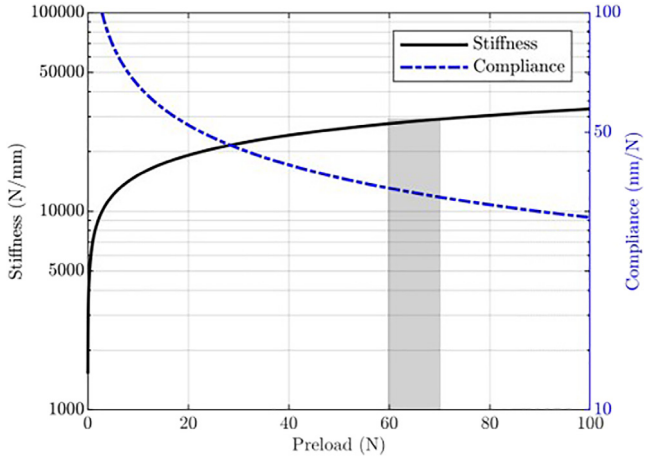

Fig. 7. Stiffness and compliance curves of one contact patch. Each kinematic joint has a preload between 60 N - 70 N.

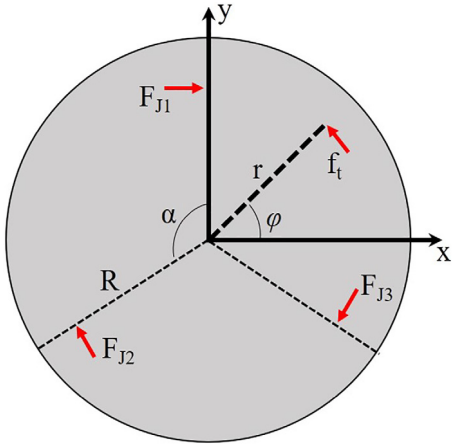

Fig. 8. A freebody diagram of the tangential tool force and the reaction forces at each kinematic joint. R is the radius of the optic, ϕ is the angle of the tool force projected from the x-axis, and α is the angle between kinematic joints, which is set to 120°.

While the magnitudes of the process forces for diamond turning and micro-grinding will differ, the force component model will hold true for both.

The general case for two deformable bodies in contact was used to calculate the deflection, the contact patch size, and the stress [17]. The slope of the deflection as a function of preload determined the stiffness and compliance curves of the contact patch, Eq. (1) and Eq. (2):

$$\delta(P) = \lambda \sqrt[3]{\frac{P^2 C_e^2}{R_e}} \tag{1}$$

$$c(P) = \frac{1}{k(P)} = \frac{2\lambda}{3P} \sqrt[3]{\frac{P^2 C_e^2}{R_e}}. \tag{2}$$

Here P is the groove normal component of the preload force, R_e is effective radius, C_e is the reciprocal of equivalent modulus, and λ is the Hertz coefficient with respect to the angle between the normal planes. Fig. 7 shows the stiffness and compliance curves for the mount as designed.

The mount was designed to have a maximum compliance at each joint during manufacturing of $65\,\mathrm{nm\,N^{-1}}$ at any radial or azimuthal location on the optical surface. During manufacturing, the tangential cutting force, which is calculated by a cutting coefficient and the chip area, shown in Eq. (3) is parallel to the preload force:

$$F_t = k_t f d, \tag{3}$$

where k_t is tangential specific cutting energy, f is feed per revolution, and d is depth of cut. The process forces are projected into the grooves of the kinematic mount, thus, the forces have a direct effect on the preload and stiffness of the joint. A diagram of the parallel forces are shown in Fig. 8. The preload vector is oriented in the same direction as the cutting force to nominally sum the forces as a function of azimuthal angle. Eqs. (4)–(6) represent the change in effective preload due to the tangential tool force as a function of the position on the optical surface, at which the cutting force is applied:

$$F_{J1}(r,\phi) = \frac{F_t r}{3L}(1 + 2\sin(\phi)) \tag{4}$$

$$F_{J2}(r,\phi) = \frac{F_t r}{3L}(1 - \sin(\phi) - \sqrt{3}\cos(\phi)) \tag{5}$$

$$F_{J3}(r,\phi) = \frac{F_t r}{3L}(1 - \sin(\phi) + \sqrt{3}\cos(\phi)). \tag{6}$$

Here L is radius of the kinematic mount circle, r is radial distance from the coupling centroid, and ϕ is azimuthal angle about the coupling centroid.

Fig. 9 shows the result of the change in preload due to a 1 N cutting force at each of the 3 joints as a function of azimuthal angle and radius, noting that the radius of force application may be greater than the radius of the coupling. The phase shift between the angle at which the peaks occur is 120°, equal to the angular separation between the coupling joints. When the cutting force is directly over one joint, the reaction force is maximum and the force at the other joints become zero.

The change in preload as a function of radius and angle is expanded into normal components of the groove for each joint. Considering the force normal to the optical surface is a fraction of the tangential component,

$$F_n = k_n f d \approx \mu F_t, \tag{7}$$

the change in reaction forces at each groove normal is found in Eq. (8) and Eq. (9):

$$F_{G1_i}(r,\phi)_{\,i=1,2,3} = F_{Ji}\frac{\cos(\theta) - \mu\sin(\theta)}{\sin(2\theta)} \tag{8}$$

$$F_{G2_i}(r,\phi)_{\,i=1,2,3} = F_{Ji}\frac{\cos(\theta) + \mu\sin(\theta)}{\sin(2\theta)}. \tag{9}$$

Here F_{Ji} is the magnitude of the resolved force at each joint and θ is the half angle of the joint vee groove.

Fig. 10 shows the result of the reaction forces from Eqs. (8) and (9). The lower groove (groove 2 in Fig. 10) has a higher reaction force than the upper groove due to the 90 degree rotation of the joints. These force changes can be substituted into Eq. (1) or (2) as a δP to calculate the positional change of the ball or the change in joint stiffness. The maximum reduction in stiffness occurs when the tool position is directly between two grooves. At this position, the preload is reduced 0.6 the resolved force at the groove, 180 degrees from the tool. The mount maintains compliance specification for a resolved tool force up to 70 N.

3. Repeatability testing

3.1. Metrology setup

Five capacitance gauges were used to measure the repeatability of the mount in the three linear and two rotational degrees of freedom. A Lion Precision Elite Series MM190 capacitance gauge system was used to record the measurements. The capacitance gauges have a resolution of 10 nm. Two gauges were placed in plane of the mount to measure $x-y$ position. Three gauges were placed underneath the mount, equilaterally spaced, allowing for axial and angular measurements. A schematic representation of the metrology loop is shown in Fig. 11. Fixturing

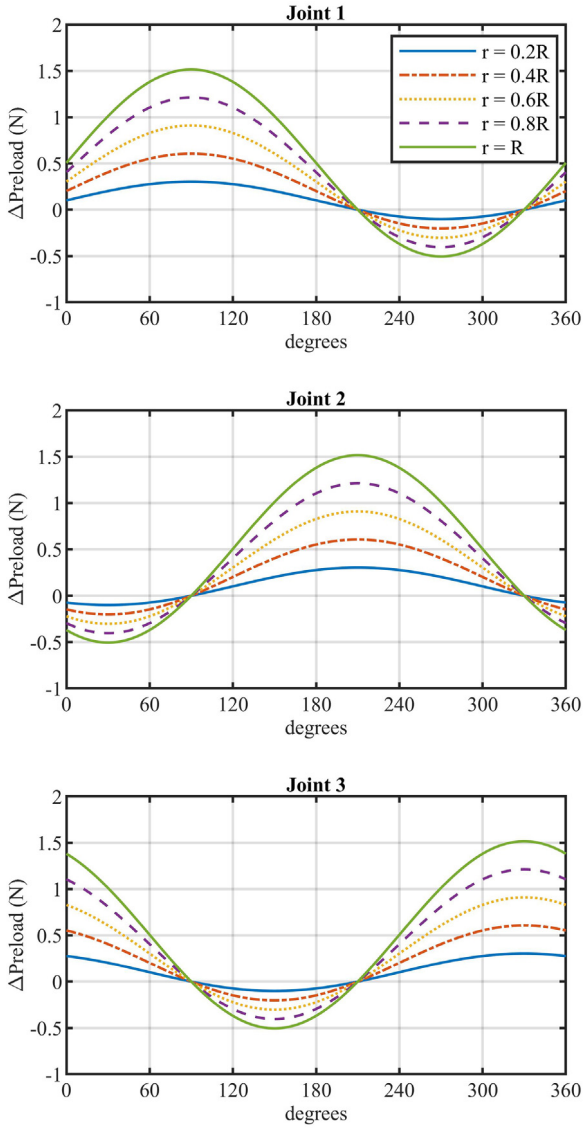

Fig. 9. Change in preload (F_{Ji}) due to cutting forces as a function of radius and azimuthal angle ϕ. R is the radius of the optic.

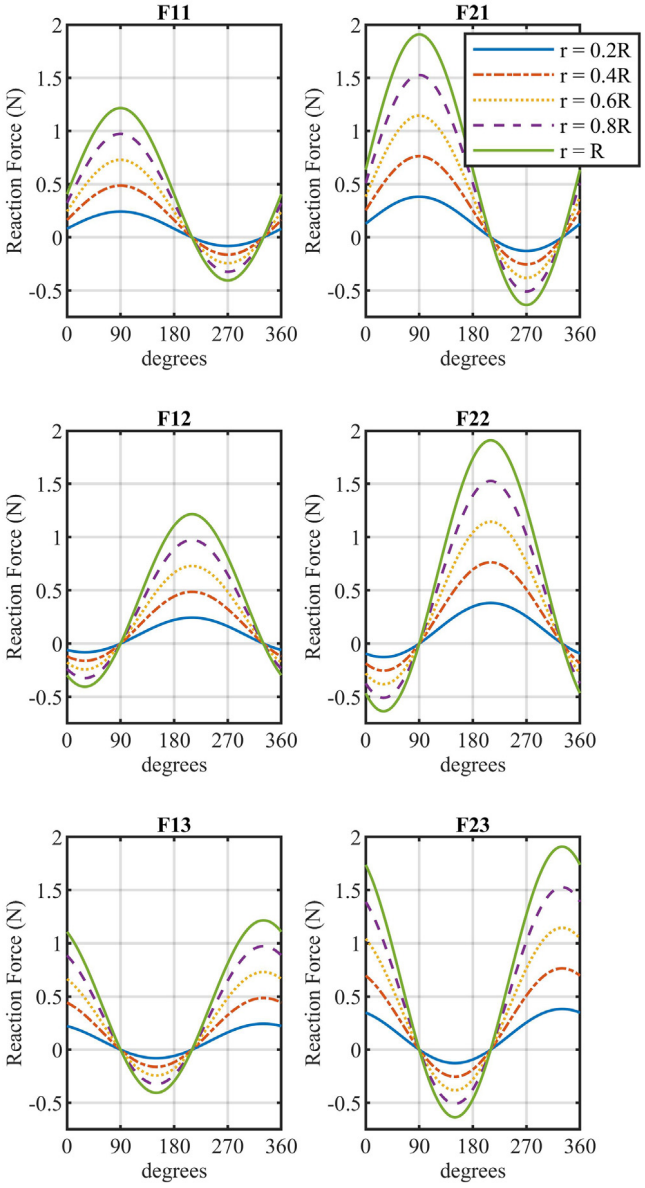

Fig. 10. Groove normal reaction forces due to cutting forces as a function of radius and azimuthal angle ϕ (F_{ij} : i =groove number, j =joint number).

was designed and fabricated out of MIC6 tooling plate to hold the five capacitance gauges, shown in Fig. 12.

The test artifact was a 270 mm aluminum optic, prior to diamond turning. Temperature sensors were placed on the outer diameter of the test artifact and fixturing. The measurements were performed on an optical bench in a temperature controlled lab with temperature stability of 0.1 °C. The metrology loop was checked for hysteresis and stability over time, prior to taking measurements.

Measurements were taken in sets of 25 and temperature data was recorded each set. The process for each trial was as follows:

1. Optic installed in mount
2. Preload applied in a sequence
3. Capacitance gauge readings recorded
4. Preload removed in a sequence
5. Optic uninstalled from mount

3.2. Absolute repeatability

An initial set of measurements were taken with no lubrication on the mount contact surfaces, which showed a break-in period at approximately 10 trials, shown in Fig. 13. The magnitude of the centroid absolute position during the break in period changed by approximately 1 μm. The measurements then settled to a peak to valley range of 0.5 μm after break in. The axial and angular changes exhibited a similar trend as the centroid position, where after the break in period the peak to valley changes were less than 0.25 μm and 2.0 μrad, respectively.

After the break in set was completed, the mount was cleaned and lubricated with a silicon based lubricant to reduce the frictional effects prior to the remaining measurements. Fig. 14 shows a typical result from a measurement set without removing the contribution of thermal drift in the data. The peak to valley range from the initial absolute position for a combined in plane repeatability is less than 200 nm. The peak to valley of the axial displacements is less than 40 nm and angular changes are less than 1 μrad.

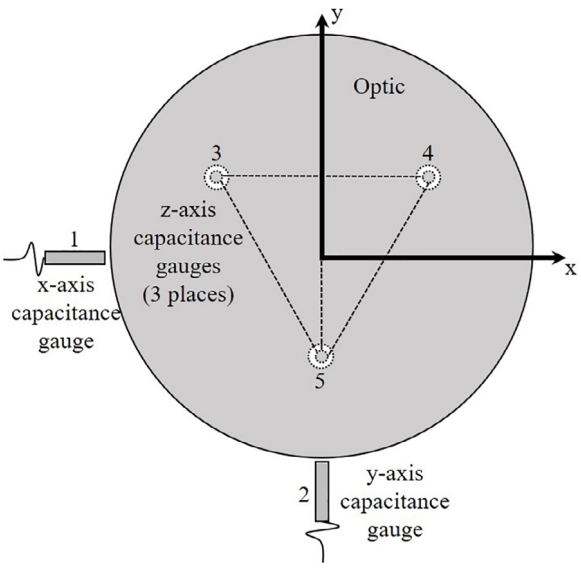

Fig. 11. A representation of the metrology configuration, where gauges 1 and 2 provide measurements for in-plane (x-y) radial positioning. The average of gauges 3, 4, and 5 provide the axial (z) positioning. Readings from gauges 3 and 4 and the distance between them, with a small angle approximation, provide rotation about the *y*-axis. The average of 3 and 4 with the reading from 5 and the distance of the bisector provides the rotation about the *x*-axis.

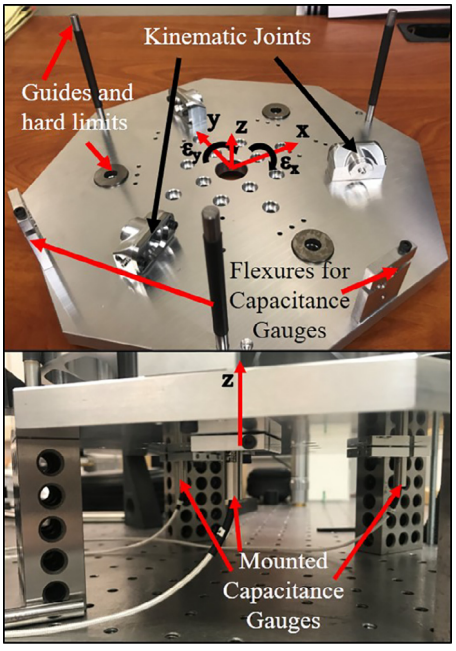

Fig. 12. The metrology frame, which contains five capacitance gauge flexure mounts and safety limits. The guide rails on the fixture and hard washer limits above the axial gauges, ensured the optic would not touch the capacitance probes during the installation.

The measurement along the *y* direction had the largest amount of drift in the data. The optic was handled closest to this sensor during the measurement process and some thermal drift was expected. Fig. 15 shows a qualitative correlation between the temperature of the metrology loop and the drift in the *y* direction measurements.

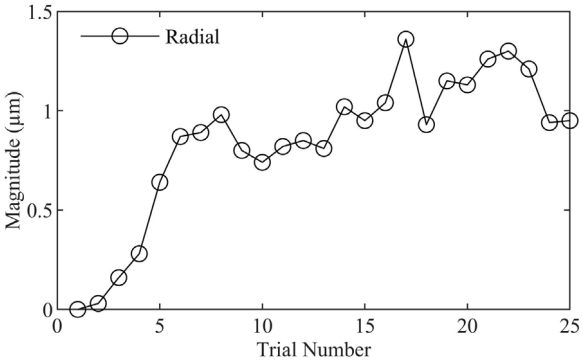

Fig. 13. This figure shows the initial radial position change of the centroid of the optic, which shows a break in period near 10 trials. The other degrees of freedom that were measured exhibited a similar effect. The measurements were taken again after the break in period, which were the measurements used to quantify the uncertainty of position repeatability.

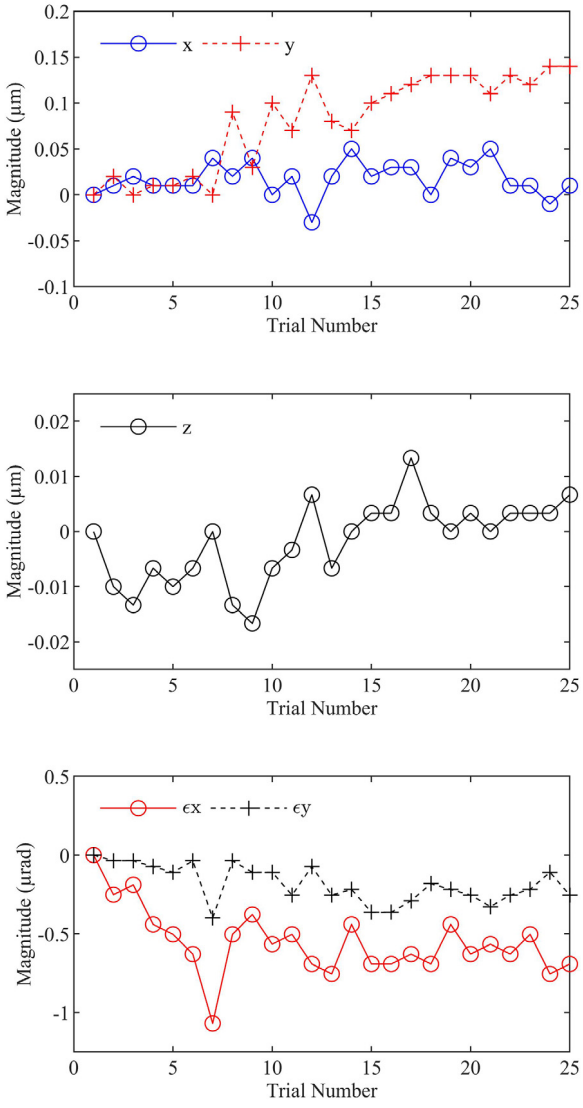

Fig. 14. Single measurement set with typical results. Temperature effects were not removed from data.

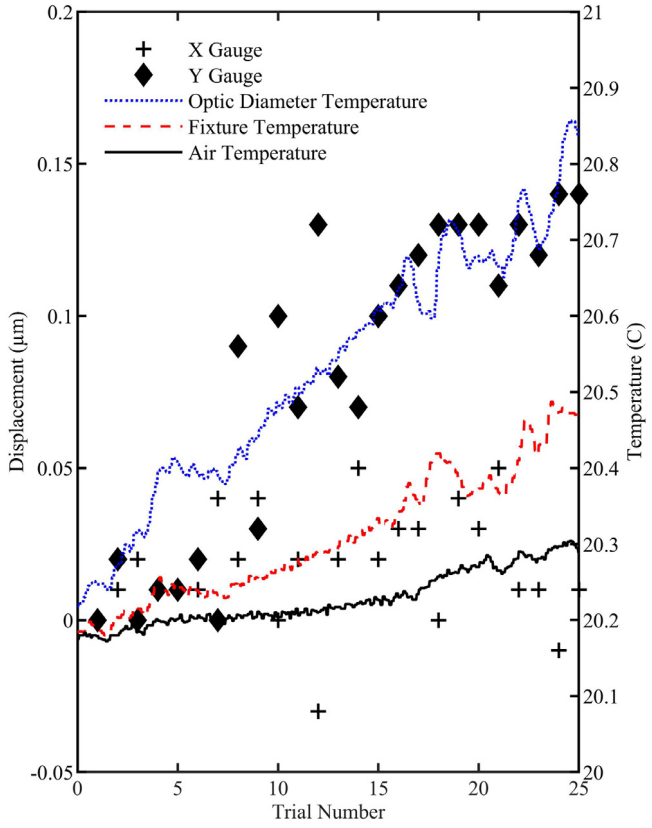

Fig. 15. The figure shows recorded temperature data overlapped with the measurements for *x,y* position repeatability. The temperature probe on the optic diameter was nearest to the Y capacitance gauge. This location on the optic is where it was handled during the repeatability test, therefore some thermal drift was expected. This thermal effect would not occur during manufacturing, as the optic and diamond turning machine will have a soak out time prior to machining.

3.3. Relative position change

The peak to valley repeatability over a series of consecutive measurements exceed the requirement by an order of magnitude, yet it is not the best representation of the mount when used in practice. In use, the optic is installed in the mount, preloaded, and the optical surface and reference datums are manufactured. The optic is removed from the mount and installed on a matched coupling for figure metrology. After figure metrology is performed, another iteration of figure correction is performed, and the process is repeated until convergence is achieved. The iterative process redefines the coordinate system of the optic after each installation with the exception of the final iteration. Therefore, the change in relative position is a direct representation of the errors that will affect system performance.

To quantify this, the absolute value of the differences between the positions from one to the next were calculated. Multiple sets of measurement data were combined with the difference taken from one measurement to the next. This gives the relative position change of the measurands. The method also reduces the uncertainty of thermal contribution from handling the optic that would otherwise not be part of the manufacturing and metrology process. The relative position change for multiple repetitions are plotted in Fig. 16. Box and whisker plots of the relative position change are shown in Fig. 17. The mean in plane relative position change is less than 50 nm for 1σ and less than 100 nm for 3σ. The mean axial relative position change is less than 10 nm and the angular changes are less than 0.25 μrad with 3σ being approximately 25 nm and 0.5 μrad respectively. Table 2 provides a summary of the results compared to the original error allowance. Table 2 also shows the updated values for the error budget, where a coverage factor was applied to the statistics from the measurements. These values are used for all each mirror in the system level error budget.

Table 2
Repeatability contribution to the error budget and a summary of the results.

Parameters	x (μm)	y (μm)	z (μm)	ϵ_x (μrad)	ϵ_y (μrad)
Initial error allowance	1.00	1.00	1.00	10.00	10.00
Absolute P-V	0.10	0.15	0.03	1.10	0.40
Relative P-V	0.06	0.10	0.03	0.60	0.60
Updated error allowance	0.15	0.15	0.06	1.25	1.25

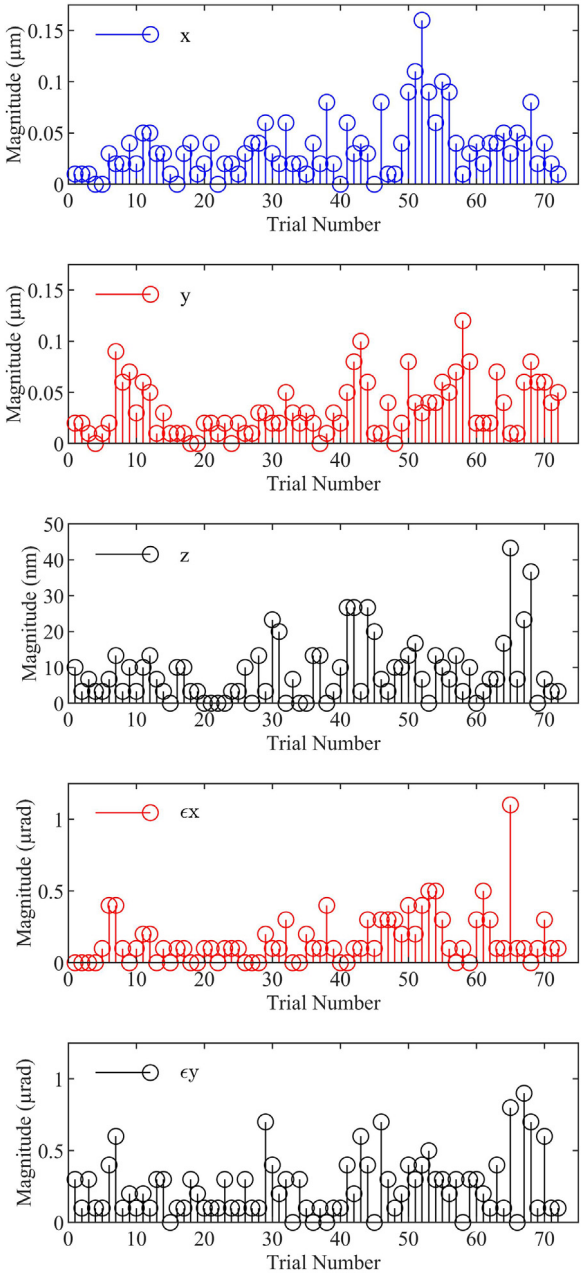

Fig. 16. Relative 5 degree of freedom repeatability magnitudes.

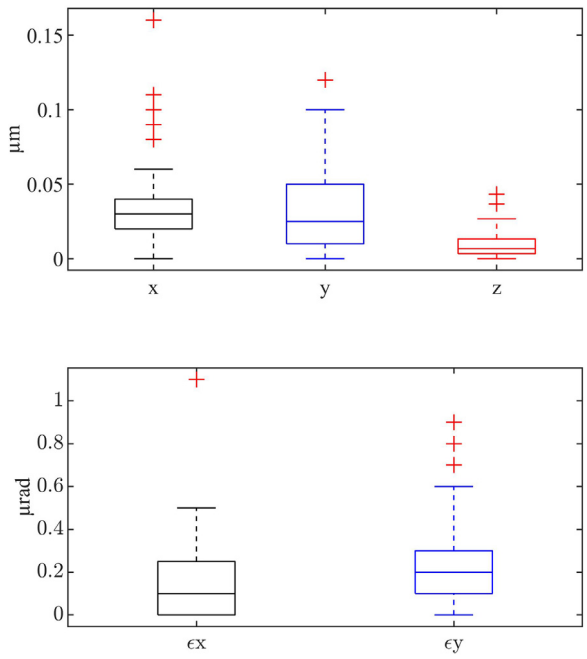

Fig. 17. Relative position changes for in plane, axial, and angular. The box represents between the 25th and 75th percentile, the line through the box is the mean value, and the whisker extensions are the peak to valley values, excluding outliers which are marked with a (+).

4. Conclusion

The kinematic mount designed and analyzed in this research meets the requirements for all expected external load cases and has a repeatability that is an order of magnitude better than the requirement. The subcomponents required no special tooling, machines or fixturing to manufacture nor did they require better than standard machining tolerances to achieve the goals. This resulted in a low cost mount where any quality machine shop could manufacture the components. The torsional preload configuration and analysis of the process forces shows the robustness of the mount, where the compliance goal was satisfied for larger cutting forces than seen in diamond turning. With an increase in preload, other machining processes and components could benefit from this type of mount, such as grinding hubs, lathe chucks, or other rotating equipment.

Declaration of competing interest

The authors declare that they have no known competing financial interests or personal relationships that could have appeared to influence the work reported in this paper.

Acknowledgments

The authors thank Dr. Chris Evans and Dr. Jimmie Miller for their input during the design process and the use of CPM lab space and equipment to perform the repeatability testing. This research was supported by the National Science Foundation I/UCRC Center for Freeform Optics, USA (IIP-1338877, IIP-1338898, IIP-1822049 and IIP-1822026).

References

[1] Reimers J, Bauer A, Thompson KP, Rolland JP. Freeform spectrometer enabling increased compactness. Light Sci Appl 2017;6(7). http://dx.doi.org/10.1038/lsa.2017.26.

[2] Fang FZ, Zhang XD, Weckenmann A, Zhang GX, Evans C. Manufacturing and measurement of freeform optics. CIRP Annals Manuf Technol 2013;62:823–46. http://dx.doi.org/10.1016/j.cirp.2013.05.003.

[3] Hoogstrate AM, van Drunen C, van Venrooy B, Henselmans R. Manufacturing of high-precision aspherical and freeform optics. Proc SPIE 2012;8450:84502Q1–9. http://dx.doi.org/10.1117/12.926040.

[4] Zhang X, Zeng Z, Liu X, Fang F. Compensation strategy for machining optical freeform surfaces by the combined on- and off- machine measurement. Opt Express 2015;23(19):24800–10. http://dx.doi.org/10.1364/OE.23.024800.

[5] Slocum AH. Kinematic couplings for precision fixturing Part I: Formulation of design parameters. Precis Eng 1988;10(2):85–91.

[6] Slocum A. Kinematic couplings: A review of design principles and applications. Int J Mach Tools Manuf 2009;50(2010):310–27. http://dx.doi.org/10.1016/j.ijmachtools.2009.10.006.

[7] Culpepper ML. Design of quasi-kinematic couplings. Precis Eng 2004;28(3):338–57. http://dx.doi.org/10.1016/j.precisioneng.2002.12.001.

[8] Willoughby PJ, Hart AJ, Slocum AH. Experimental determination of kinematic coupling repeatability in industrial and laboratory conditions. J Manuf Syst 2005;24(2):108–21.

[9] Hale LC, Slocum AH. Optimal design techniques for kinematic couplings. Precis Eng 2001;25:114–27.

[10] Slocum A. Design of three groove kinematic couplings. Precis Eng 1992;14(2):67–76.

[11] Kruis JRCG. Design, analysis, testing and applications of two-body and three-body kinematic mounts [Ph.D. thesis], Ecole Polytechnique Federale De Lausanne; 2016.

[12] Schmiechen P, Slocum A. Analysis of kinematic systems: a generalized approach. Precis Eng 1996;19(1):11–8.

[13] Hale LC. Principles and Techniques for Designing Precision Machines [Ph.D. thesis], MIT; 1999.

[14] Barraja M, Ryan Vallance R. Tolerancing kinematic couplings. Precis Eng 2005;29:101–12. http://dx.doi.org/10.1016/j.precisioneng.2004.05.001.

[15] Horvath NW, Davies MA. Concurrent engineering of a next-generation freeform telescope: mechanical design and manufacture. In: Advanced optics for imaging applications: UV through LWIR IV (vol. 10998). SPIE; 2019, p. 1–8. http://dx.doi.org/10.1117/12.2518954.

[16] Brinksmeier E, Mutlugünes Y, Klocke F, Aurich J, Shore P, Ohmori H. Ultra-precision grinding. CIRP Annals 2010;59(2):652–71. http://dx.doi.org/10.1016/J.CIRP.2010.05.001.

[17] Young WC, Budynas RG. Roark's formulas for stress and strain. 8th ed. McGraw-Hill; 2012.